

H₂BZmacropa-NCS: A Bifunctional Chelator for Actinium-225 Targeted Alpha Therapy

Karthika J. Kadassery,[§] A. Paden King,[§] Stanley Fayn, Kwamena E. Baidoo, Samantha N. MacMillan, Freddy E. Escorcía,* and Justin J. Wilson*



Cite This: *Bioconjugate Chem.* 2022, 33, 1222–1231



Read Online

ACCESS |



Metrics & More

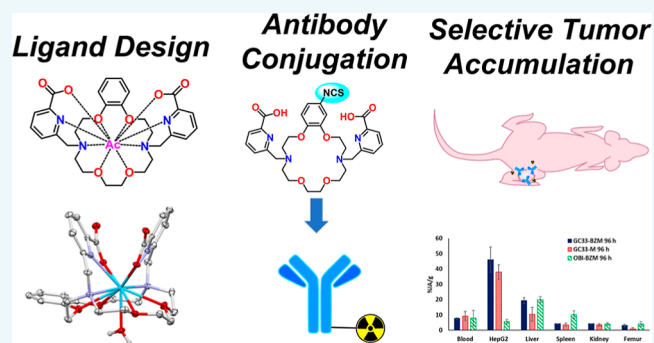


Article Recommendations



Supporting Information

ABSTRACT: Actinium-225 (²²⁵Ac) is one of the most promising radionuclides for targeted alpha therapy (TAT). With a half-life of 9.92 days and a decay chain that emits four high-energy α particles, ²²⁵Ac is well-suited for TAT when conjugated to macromolecular targeting vectors that exhibit extended in vivo circulation times. The implementation of ²²⁵Ac in these targeted constructs, however, requires a suitable chelator that can bind and retain this radionuclide in vivo. Previous work has demonstrated the suitability of a diaza-18-crown-6 macrocyclic chelator H₂macropa for this application. Building upon these prior efforts, in this study, two rigid variants of H₂macropa, which contain either one (H₂BZmacropa) or two (H₂BZ₂macropa) benzene rings within the macrocyclic core, were synthesized and investigated for their potential use for ²²⁵Ac TAT. The coordination chemistry of these ligands with La³⁺, used as a nonradioactive model for Ac³⁺, was carried out. Both NMR spectroscopic and X-ray crystallographic studies of the La³⁺ complexes of these ligands revealed similar structural features to those found for the related complex of H₂macropa. Thermodynamic stability constants of the La³⁺ complexes, however, were found to be 1 and 2 orders of magnitude lower than those of H₂macropa for H₂BZmacropa and H₂BZ₂macropa, respectively. The decrease in thermodynamic stability was rationalized via the use of density functional theory calculations. ²²⁵Ac radiolabeling and serum stability studies with H₂BZmacropa showed that this chelator compares favorably with H₂macropa. Based on these promising results, a bifunctional version of this chelator, H₂BZmacropa-NCS, was synthesized and conjugated to the antibody codrituzumab (GC33), which targets the liver cancer biomarker glypican-3 (GPC3). The resulting GC33-BZmacropa conjugate and an analogous GC33-macropa conjugate were evaluated for their ²²⁵Ac radiolabeling efficiencies, antigen-binding affinities, and in vivo biodistribution in HepG2 liver cancer tumor-bearing mice. Although both conjugates were comparably effective in their radiolabeling efficiencies, [²²⁵Ac]Ac-GC33-BZmacropa showed slightly poorer serum stability and biodistribution than [²²⁵Ac]Ac-GC33-macropa. Together, these results establish H₂BZmacropa-NCS as a new bifunctional chelator for the preparation of ²²⁵Ac radiopharmaceuticals.



INTRODUCTION

The 2013 FDA approval of ²²³RaCl₂ (Xofigo) for the management of bone metastases in castration-resistant prostate cancer patients has heralded a renaissance in targeted alpha therapy (TAT), a treatment modality that uses the high linear energy transfer of alpha (α) particles to annihilate cancer cells.¹ Despite the success of this drug, the development of new radiopharmaceutical agents employing ²²³Ra has been hindered by the difficult chelation chemistry of this ion.² Fortunately, a number of other α -emitting radionuclides, such as ²²⁷Th, ²²⁵Ac, ²¹³Bi, ²¹²Bi, ²¹²Pb, and ²¹¹At, have suitable properties for use in TAT.³ Among these radionuclides, ²²⁵Ac has demonstrated particular promise due to advances in its large-scale production, its ideal 9.92-day physical half-life for conjugation to long-lived biomolecules, and its high cytotoxic potency, which arises from the four α particles emitted through its decay chain.^{4,5} Clinical

trials of ²²⁵Ac small-molecule^{6,7} and antibody⁸ conjugates are underway, and early results have been promising.

A significant limitation in the development of new ²²⁵Ac-based TAT radiopharmaceutical agents has arisen from the difficulty in identifying suitable chelating agents for the large Ac³⁺ ion.⁵ Although acyclic chelators such as ethylenediamine tetraacetic acid (H₄EDTA) and diethylenetriamine pentaacetic acid (H₅DTPA) have been shown to possess high affinity for the ²²⁵Ac³⁺ ion, the resulting complexes are labile, leading to the

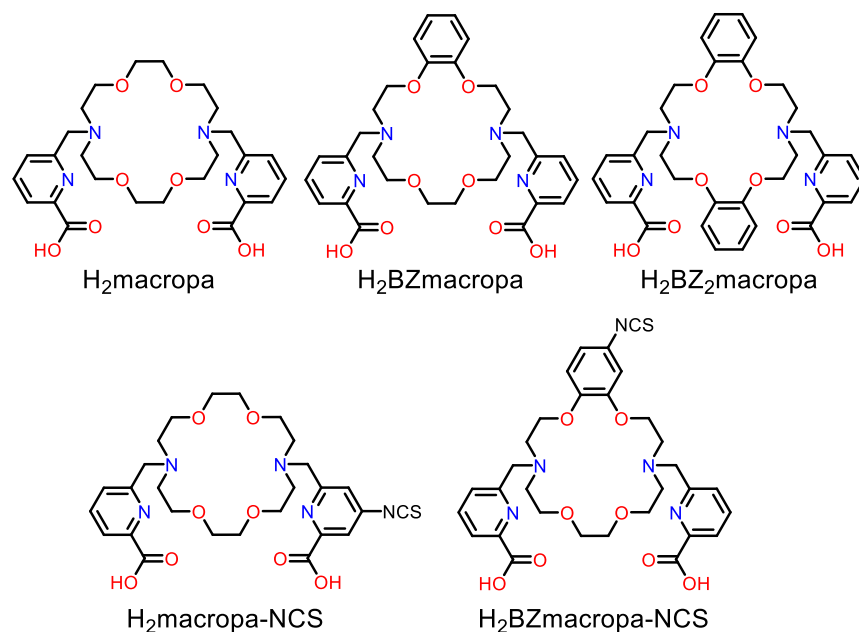
Received: April 20, 2022

Revised: May 19, 2022

Published: June 7, 2022



Chart 1. Chelators Discussed in This Work



release of the free metal ion in biological systems.⁹ By contrast, many Ac^{3+} complexes of macrocyclic chelators are substantially more inert. For example, the macrocyclic chelator tetraazacyclododecane-1,4,7,10-tetraacetic acid (H_4DOTA) has been used successfully for both small-molecule and antibody ^{225}Ac -radioconjugates, albeit with some significant challenges. For example, radiolabeling of H_4DOTA with ^{225}Ac either requires high temperatures, which are incompatible with macromolecular biomolecules such as antibodies, or long incubation times, which yields constructs with relatively low specific activities.^{10–14} Furthermore, serum stability studies have shown that the $[\text{}^{225}\text{Ac}]\text{Ac-DOTA}$ complex dissociates over time,¹⁵ a property that is corroborated by animal studies that show deposition of ^{225}Ac in the liver and femur after the administration of DOTA-based conjugates.¹⁶ These drawbacks have sparked efforts to develop superior bifunctional chelators for ^{225}Ac .

To accommodate the large ionic radius of Ac^{3+} , researchers have targeted alternative ligands that contain more than eight donor atoms to saturate its coordination sphere. For instance, macrocycles bispa,¹⁷ crown,¹⁸ macrodipa, and py-macrodipa,¹⁹ as well as acyclic chelators octapa,¹⁵ py4pa,²⁰ and phospho,¹⁵ have all successfully radiolabeled $^{225}\text{Ac}^{3+}$ at room temperature in <60 min. However, not all these chelators form sufficiently stable complexes with ^{225}Ac for biological use.

Among the potential alternatives to H_4DOTA , the diaza-18-crown-6 macrocyclic chelator $\text{H}_2\text{macropa}$ (Chart 1) has shown significant promise for ^{225}Ac chelation in TAT applications.^{24,25} This compound is unique by virtue of its high selectivity for large over small lanthanide ions,²¹ a property that makes it favorable for use with the large Ac^{3+} ion. In contrast to H_4DOTA , this chelator can quantitatively radiolabel ^{225}Ac at room temperature in 5 min and form complexes that are sufficiently stable for long-term biological applications. The success of this chelator with ^{225}Ac has been demonstrated by several studies that have used it in conjunction with small-molecule and antibody-based targeting vectors.^{26–29}

The efficacy of $\text{H}_2\text{macropa}$ suggests that this structural archetype is valuable for Ac^{3+} chelation. Building upon this

scaffold, two new analogues of $\text{H}_2\text{macropa}$ were investigated. These compounds are rigidified versions of the parent chelator, containing either one ($\text{H}_2\text{BZmacropa}$) or two ($\text{H}_2\text{BZ}_2\text{macropa}$) benzene rings within the 18-membered macrocycle (Chart 1). We hypothesized that the decreased conformational flexibility of these new analogues would preorganize them for more effective and stable chelation of the Ac^{3+} ion.^{30–35} This study presents a comprehensive comparative investigation of these new chelators with respect to their La^{3+} - and Ac^{3+} -complexing properties. Furthermore, a bifunctional chelator, $\text{H}_2\text{BZmacropa-NCS}$, and its conjugate to the glypican-3 (GPC3)-targeting antibody codrituzumab³⁶ (GC33) were prepared. The resulting ^{225}Ac -labeled GC33-BZmacropa conjugate was then assessed in an in vivo mouse model of liver cancer. Collectively, the results from this study highlight the importance of ligand design principles in developing effective chelating agents for TAT applications.

RESULTS AND DISCUSSION

Chelator Syntheses. The previously reported ligands, $\text{H}_2\text{macropa}$ ²¹ and $\text{H}_2\text{BZmacropa}$,³⁷ and the novel ligand $\text{H}_2\text{BZ}_2\text{macropa}$ were synthesized via adaptations of procedures that have been used to access related macrocyclic chelators.³⁸ Briefly, the ligands were synthesized via the alkylation of the corresponding diaza-18-crown-6 macrocycle at the secondary amine nitrogen with 6-(bromomethyl)pyridine-2-carboxylic acid methyl ester, followed by acid hydrolysis of the ester functional groups (Schemes S1 and S2). The ligands were fully characterized using NMR spectroscopy, mass spectrometry (MS), elemental analysis, and analytical high-performance liquid chromatography (HPLC) (Figures S1–S29).

Coordination Chemistry with La^{3+} . Because no stable isotopes of Ac^{3+} exist, the coordination chemistries of $\text{H}_2\text{BZmacropa}$ and $\text{H}_2\text{BZ}_2\text{macropa}$ were investigated using La^{3+} . As the largest lanthanide, this ion has a similar ionic radius, hydrolysis constant, and hard–soft acid–base properties to Ac^{3+} , thus rendering it a suitable model.^{5,39} Treatment of equimolar ratios of LaCl_3 with each compound in water at neutral pH followed by salt metathesis with KPF_6 led to the precipitation of the $[\text{LaL}(\text{H}_2\text{O})]\text{PF}_6$ complexes, which were

crystallized via the slow evaporation of concentrated aqueous solutions at room temperature. The structures of these complexes (Figure 1), as determined using X-ray crystallog-

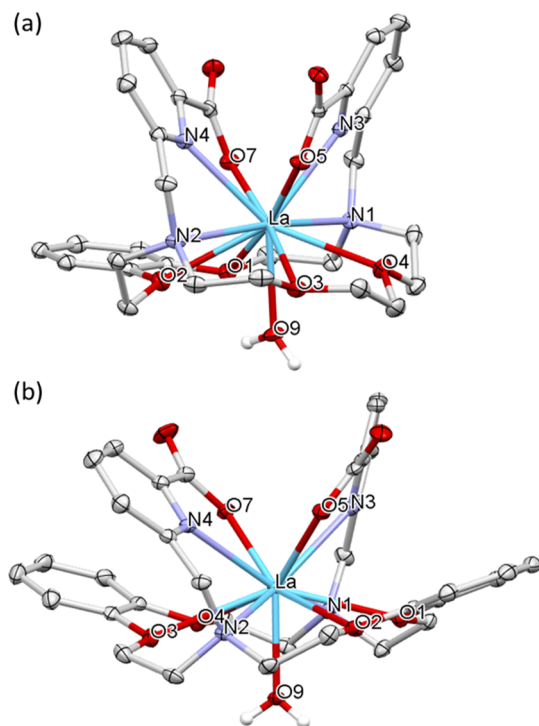


Figure 1. Crystal structures of (a) $[\text{La}(\text{BZmacropa})(\text{H}_2\text{O})](\text{PF}_6)$ and (b) $[\text{La}(\text{BZ}_2\text{macropa})(\text{H}_2\text{O})](\text{PF}_6)$. Thermal ellipsoids are drawn at the 50% probability level. Outer-sphere solvents, counter-anions, and hydrogen atoms attached to carbon centers are omitted for clarity. Color scheme: La = teal; O = red; N = blue; and C = gray.

raphy, are comparable to that of $[\text{La}(\text{macropa})(\text{H}_2\text{O})]^+$.²⁴ In all three complexes, the La^{3+} center attains an 11-coordinate geometry with 10 donors provided by the macrocyclic ligands and the 11th arising from an inner-sphere water molecule that interpenetrates the macrocyclic core.

Within the macropa^{2-} and BZmacropa^{2-} structures, the metal ion sits above the mean plane of the O atoms in the macrocycle (O1–O4), resulting in near linear N1–La–N2 angles of 178.04 and 172.41°, respectively. By contrast, the structure of $[\text{La}(\text{BZ}_2\text{macropa})(\text{H}_2\text{O})]^+$ shows that all the donor atoms of the macrocyclic base reside in a plane below the La^{3+} center,

rendering the N1–La–N2 angle to be much more acute (148.77°). This distortion is most likely a consequence of the presence of the two rigid benzene groups, which lead to additional strain in the macrocycle of $\text{BZ}_2\text{macropa}^{2-}$ upon coordination to the La^{3+} backbone.

In addition to this distortion, there are also significant differences with respect to the interatomic distances between the donor atoms and the La^{3+} center within these structures. For example, the inner coordination sphere of the La^{3+} ion in the BZmacropa complex is relatively asymmetric; the La–N distances on the macrocycle are 2.857 and 2.957 Å, representing a significant difference of 0.1 Å. Furthermore, the La–O distances from the aryl ether oxygens of the macrocycle are significantly disparate at 2.772 and 3.058 Å. By contrast, the crystal structure of $[\text{La}(\text{BZ}_2\text{macropa})(\text{H}_2\text{O})]^+$ is relatively symmetric with chemically equivalent donor atoms interacting with the La^{3+} center at similar distances. However, the La–O distances within the macrocycle fall between 2.83 and 2.96 Å. By contrast, the crystal structure of $[\text{La}(\text{macropa})]^+$ has La–O distances that are much shorter (between 2.70 and 2.79 Å). Thus, the aryl ethers donors conferred by the benzene ring appear to interact more weakly than the aliphatic ethereal donors, as evidenced by the longer interatomic distances in the former.

Solution Thermodynamics with La^{3+} . To assess the effects of the presence of the rigid benzene groups on the metal-binding properties of $\text{H}_2\text{BZmacropa}$ and $\text{H}_2\text{BZ}_2\text{macropa}$, the thermodynamic stabilities of their La^{3+} complexes were measured via pH potentiometric titrations. The protonation constants of $\text{H}_2\text{BZmacropa}$ and $\text{H}_2\text{BZ}_2\text{macropa}$ and the stability constants of their La^{3+} complexes are collected in Table 1. For both chelators, a total of four protonation constants were observed over a pH range of 2.5–11.3. The first and the second protonation constants most likely correspond to the sequential protonation of the macrocyclic amine nitrogen atoms, whereas the third and fourth protonation constants are assigned to the protonation at the picolinate pendent arms. Although there are six basic sites on the chelators, the fifth and sixth protonation constants could not be determined using the pH ranges employed in these titrations. The sum of the first and second protonation constants of the rigid compounds are 0.8 and 1.3 log units, respectively, lower than that of macropa , indicating that the addition of phenyl groups increases the acidity of the macrocycles. This result is an expected consequence of the electron-withdrawing nature of the phenyl groups and is consistent with previously reported data on similar macrocyclic

Table 1. Protonation Constants of Various Chelators and the Thermodynamic Stability Constants of Corresponding La^{3+} Complexes Determined Using pH Potentiometry (25 °C and $I = 0.1 \text{ M KCl}$)

	$\text{H}_2\text{macropa}$	$\text{H}_2\text{BZmacropa}$	$\text{H}_2\text{BZ}_2\text{macropa}$	H_4DOTA	H_3DTPA	H_4EDTA
$\log K_1$	7.41(1) ^c	7.06(2)	6.89(7)	11.14 ^d	10.45 ^e	10.17 ^e
$\log K_2$	6.85(1) ^c	6.41(1)	6.11(3)	9.69 ^d	8.53 ^e	6.11 ^e
$\log K_3$	3.32(1) ^c	3.35(2)	3.36(3)	4.84 ^d	4.28 ^e	2.68 ^e
$\log K_4$	2.36(1) ^c	2.41(9)	2.26(9)	3.95 ^d	2.65 ^e	2.00 ^e
$\log K_5$	1.69(1) ^c				1.82 ^e	1.5 ^e
$\log K_{\text{LaL}}$	14.99(2) ^c	13.99(5)	12.04(6)	21.7(1) ^d	19.48 ^e	15.46 ^e
$\log K_{\text{LaHL}}$	2.28(3) ^c			2.5(2) ^d		2.24 ^e
$\log K'_{\text{La}}$ ^a	14.63	13.81	11.92	15.67	15.27	12.67
pLa ^b	15.58	14.77	12.87	16.62	16.22	13.62

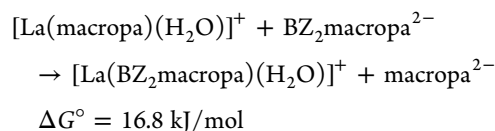
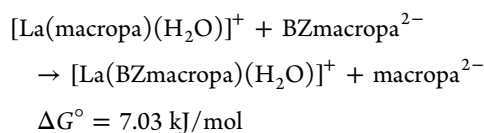
^aConditional stability constants ($\log K'_M$) at a pH of 7.4, 25 °C, and $I = 0.1 \text{ M KCl}$. ^bpM values calculated from $-\log[M]_{\text{free}}$ ($[M]_{\text{total}} = 10^{-6} \text{ M}$, $[L]_{\text{total}} = 10^{-5} \text{ M}$, pH 7.4, 25 °C, and $I = 0.1 \text{ M KCl}$). ^c0.1 M KCl, ref 21. ^d0.1 M KCl, ref 22. ^e0.1 M, ref 23.

chelators.^{40–42} It should be noted that the protonation constants for H₂BZmacropa have been previously reported,³⁷ and these values—in particular, the most basic protonation constant—differ somewhat from those measured in this study. The use of different media for ionic strength (0.1 M KCl vs 0.1 M KNO₃) could partly explain these discrepancies. In any case, the pH potentiometric titrations in the present study were carried out in triplicate and are reported with a high degree of confidence.

After obtaining the protonation constants, the La³⁺ stability constants (log *K*_{LaL}) of the H₂BZmacropa and H₂BZ₂macropa complexes were determined using pH potentiometric titrations (Table 1). The log *K*_{LaL} values decrease upon the addition of phenyl groups to the macrocyclic backbone, following the sequence log *K*_{Lamacropa} > log *K*_{LaBZmacropa} > log *K*_{LaBZ₂macropa}. The stability constant for the La³⁺ complex of H₂BZmacropa (log *K*_{LaL} = 13.99) is approximately 1 log unit lower than that of H₂macropa (log *K*_{LaL} = 14.99). The introduction of a second phenyl group in H₂BZ₂macropa leads to an even greater destabilization of the complexes, as reflected by a log *K*_{LaL} value (log *K*_{LaL} = 12.04) that is almost 2 log units lower than that of H₂BZmacropa. In order to account for the effect of protonation equilibria of the ligands on complex stability, the conditional stability constants (log *K*'_{LaL}) and pLa (the negative log of the free metal concentration in a solution containing 10^{−6} M metal ions and 10^{−5} M chelator) at a biologically relevant pH of 7.4 were calculated (Table 1). The trends in these conditional stability constants follow those of the absolute values with log *K*'_{Lamacropa} = 14.63, log *K*'_{LaBZmacropa} = 13.81, and log *K*'_{LaBZ₂macropa} = 11.92. Although ligand rigidification should in principle lead to enhanced metal complex stability, this effect may depend on several factors including the type of metal employed. For example, a previous study of ethylene glycol-bis(β-aminoethyl ether)-*N,N,N',N'*-tetraacetic acid (H₄EGTA) and an analogue of H₄EGTA with a phenyl backbone showed that enhanced stability was exhibited for the Ca²⁺ complex but that the stability decreased for the La³⁺ complex.⁴² The reduced stability observed in the cases of H₂BZmacropa and H₂BZ₂macropa may thus be a consequence of several different factors.

Although the overall LaL stability constants for the rigid ligands are lower than that of H₂macropa, the absolute values exceed 10¹⁰, suggesting that they form sufficiently strong complexes for use in ²²⁵Ac TAT.

Density Functional Theory Calculations. In order to better understand the La³⁺ stability constant trends, density functional theory (DFT) was employed. The geometries of [La(macropa)(OH₂)]⁺, [La(BZmacropa)(OH₂)]⁺, and [La(BZ₂macropa)(OH₂)]⁺ were first optimized. The resulting structures are qualitatively similar to the experimentally determined X-ray crystal structures but exhibit a systematic elongation of the La donor atom distances within the macrocycles of approximately 0.05–0.10 Å. More importantly, however, the relative asymmetry of [La(BZmacropa)(OH₂)]⁺ is captured via the DFT optimization, thus validating this level of theory. With suitably optimized structures, the Δ*G*^o values for the transchelation reaction between [La(macropa)(H₂O)]⁺ and either BZmacropa^{2−} or BZ₂macropa^{2−} were calculated.



For both of these reactions, the Δ*G*^o was found to be >0, indicating that both BZmacropa^{2−} and BZ₂macropa^{2−} form less thermodynamically stable complexes with La³⁺ than macropa^{2−}. Furthermore, Δ*G*^o for the transchelation with BZ₂macropa^{2−} was approximately 10 kJ/mol greater than that for BZmacropa^{2−}. Collectively, these computational results are consistent with our experimental data that show BZ₂macropa^{2−} forms the least stable La³⁺ complex of these three ligands.

Having validated our computational method against the experimental results, we analyzed the different factors that contribute to Δ*G*^o for these reactions. As described in the Supporting Information (Section S1.6), Δ*G*^o can be expressed as the sum ΔΔ*G*_S^o + ΔΔ*G*_B^o, where ΔΔ*G*_S^o is the relative ligand strain energy and ΔΔ*G*_B^o is the relative metal ion-binding energy (see Supporting Information Section S1.6 for more details).^{35,38,43,44} The strain energy (Δ*G*_S^o) is defined as the free energy change required to distort the geometrically relaxed free ligand (L) to a conformation that is suitable for metal ion binding (L_{strain}, eq S1), and the binding energy (Δ*G*_B^o) is defined as the free energy change associated with the incorporation of the La³⁺ ion into the ligand in its preorganized metal-binding conformation (eq S2). The relative (ΔΔ*G*) values, compared to that of macropa^{2−}, are given below.

$$\Delta\Delta G_S^\circ(\text{BZmacropa}^{2-}) = -13.95 \text{ kJ/mol}$$

$$\Delta\Delta G_B^\circ(\text{BZmacropa}^{2-}) = 20.98 \text{ kJ/mol}$$

$$\Delta\Delta G_S^\circ(\text{BZ}_2\text{macropa}^{2-}) = -14.41 \text{ kJ/mol}$$

$$\Delta\Delta G_B^\circ(\text{BZ}_2\text{macropa}^{2-}) = 31.17 \text{ kJ/mol}$$

For both BZmacropa^{2−} and BZ₂macropa^{2−}, ΔΔ*G*_S^o values are negative, indicating that these compounds undergo a significantly smaller free energy penalty for attaining an appropriate metal-binding conformation than macropa^{2−}. This result is consistent with role of the rigid benzene groups in enhancing the metal-binding preorganization of these ligands. By contrast, the ΔΔ*G*_B^o values for both rigid chelators are positive, a result that suggests that macropa forms stronger binding interactions with the La³⁺ ion. The weaker binding energies of H₂BZmacropa and H₂BZ₂macropa, compared to that of H₂macropa, is most likely a consequence of their decreased basicity and donor strength. As noted above, the electron-withdrawing phenyl groups embedded in the macrocycle decreases their basicity, as determined experimentally via protonation constant measurements. This decreased basicity also renders them less effective Lewis bases for binding with La³⁺. To further verify this conclusion computationally, the Δ*G*^o for a simple model ligand substitution reaction on La³⁺ was calculated. In this substitution reaction, the Δ*G*^o values required to displace dimethyl ether, a model for the aliphatic ether donors in H₂macropa, with anisole, an aromatic ether that models the donors on H₂BZmacropa and H₂BZ₂macropa, were calculated. These calculations revealed that the displacement of dimethyl ether by anisole is thermodynamically uphill (Δ*G*^o = 17.22 kJ/mol). Thus, the weaker donor strength of the aromatic ethers is a plausible explanation for the positive ΔΔ*G*_B^o determined for H₂BZmacropa and H₂BZ₂macropa. Together, these results

reveal a counterbalancing effect of the introduction of the rigid phenyl groups. Although these rigid phenyl groups provide a favorable entropic contribution by preorganizing the ligands for metal binding, their weaker donor strengths provide a poorer enthalpic contribution to La^{3+} binding. For BZmacropa^{2-} and $\text{BZ}_2\text{macropa}^{2-}$, the weaker binding strength outweighs the benefits obtained in ligand preorganization.

Radiolabeling and Stability Studies. Alongside the comprehensive characterization of the La^{3+} complexes of BZmacropa^{2-} and $\text{BZ}_2\text{macropa}^{2-}$, which revealed them to be effective ligands for this ion, their ability to chelate Ac^{3+} was investigated. The chelators ($\sim 300 \mu\text{M}$) were incubated at room temperature with $70 \mu\text{Ci}$ (2.6 Mbq) $[\text{}^{225}\text{Ac}]\text{Ac}(\text{NO}_3)_3$ in water containing NH_4OAc (0.1 M) at a pH of 5.5. Under these conditions, both ligands, as well as macropa, quantitatively radiolabeled $^{225}\text{Ac}^{3+}$ in only 30 min, resulting in high specific activities of approximately 7.5 Ci/g (278 GBq/g). Instant thin-layer chromatography (ITLC) chromatograms, showing the complex formation for these ligands and macropa, are shown in the Supporting Information, Figures S63–S66. These results, particularly the successful radiolabeling at room temperature, confirm the high efficacy of expanded macrocyclic ligands such as macropa^{2-} for chelation of the large Ac^{3+} ion.

Having demonstrated the rapid and high-specific-activity radiolabeling with $\text{H}_2\text{BZmacropa}$ and $\text{H}_2\text{BZ}_2\text{macropa}$, the stabilities of the resulting Ac^{3+} complexes in whole human serum at 37°C were evaluated (Figures 2 and S70–S72). Under

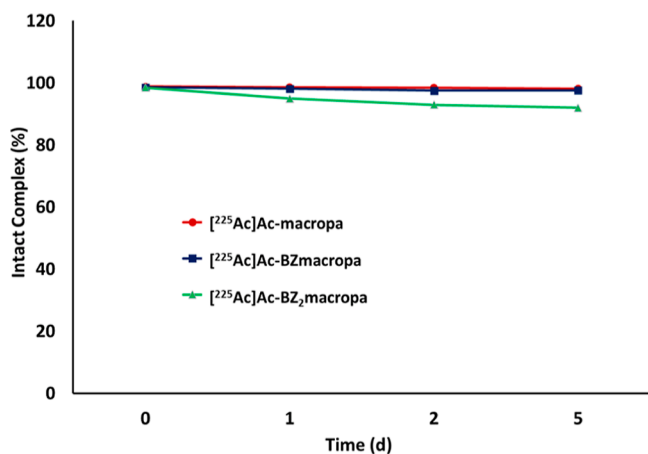


Figure 2. Stability of ^{225}Ac complexes in human serum over time. Stability was measured using ITLC condition 1, as detailed in the Supporting Information.

these conditions, all complexes were $>90\%$ intact after 5 days. Even with this high uniform stability among the complexes, several trends could be discerned. Specifically, the increase in the stability of the complexes followed the order $\text{BZ}_2\text{macropa}^{2-} < \text{BZmacropa}^{2-} < \text{macropa}^{2-}$. This trend matches that observed with the thermodynamic stability constant data of the La^{3+} complexes that was rationalized using DFT calculations, as described above.

Bifunctional Chelator $\text{H}_2\text{BZmacropa-NCS}$. The high stability of the ^{225}Ac complex of BZmacropa prompted us to prepare a bifunctional version of this chelator. For this purpose, we targeted the chelator $\text{H}_2\text{BZmacropa-NCS}$ (Chart 1), which contains an amine-reactive isothiocyanate group appended to the phenyl ring of the macrocyclic backbone. The synthesis of this compound (Scheme 1) commenced from macrocycle 3,

which upon treatment with 1 equiv of KNO_3 in trifluoroacetic acid afforded the monosubstituted nitro-product 8 in near quantitative yield. The addition of the pendent arms to the nitrated macrocycle was accomplished via alkylation of 8 at the secondary amine nitrogen with 6-(bromomethyl)pyridine-2-carboxylic acid methyl ester. Reduction of the nitrated compound 9 using H_2 over Pd/C followed by acid hydrolysis of the ester functional groups yielded $\text{H}_2\text{BZmacropa-NH}_2$. Finally, the isothiocyanate functional group was installed onto the macrocycle via the treatment of $\text{H}_2\text{BZmacropa-NH}_2$ with excess thiophosgene. Compound $\text{H}_2\text{BZmacropa-NCS}$ was fully characterized using NMR spectroscopy, MS, and analytical HPLC (Figures S30–S40).

A key difference between the first-generation bifunctional chelator $\text{H}_2\text{macropa-NCS}$ (Chart 1) and $\text{H}_2\text{BZmacropa-NCS}$ is the location of the amine-reactive $-\text{NCS}$ group. On $\text{H}_2\text{BZmacropa-NCS}$, this functional group is attached to the macrocycle backbone, whereas for $\text{H}_2\text{macropa-NCS}$, it is on one of the picolinate pendent arms. Consequently, the synthesis of $\text{H}_2\text{BZmacropa-NCS}$ is more modular in that it proceeds through intermediate 8, which can potentially be functionalized with a diverse range of different pendent donor arms to access a library of different bifunctional chelators. Furthermore, $\text{H}_2\text{BZmacropa-NCS}$ is relatively easier to synthesize as compared to $\text{H}_2\text{macropa-NCS}$. For instance, the synthesis of $\text{H}_2\text{macropa-NCS}$ involves a nine-step pathway starting from the macrocycle, while the synthesis of $\text{H}_2\text{BZmacropa-NCS}$ is carried out in four or five steps. The location of the $-\text{NCS}$ functional group also has important effects on its hydrolytic stability. For instance, a solution of $\text{H}_2\text{macropa-NCS}$ in pH 9.1 NaHCO_3 buffer at room temperature completely hydrolyzes to amine $\text{H}_2\text{macropa-NH}_2$ in approximately 5 h ($t_{1/2} = 1.25 \text{ h}$). Under the same conditions, the hydrolysis of $\text{H}_2\text{BZmacropa}$ is significantly slower ($t_{1/2} = 56 \text{ h}$), requiring over a week for near complete formation of the amine. The location of the $-\text{NCS}$ group of $\text{H}_2\text{macropa-NCS}$ directly on the electron-deficient picolinate group increases its electrophilicity, rendering it more reactive and less stable than the $-\text{NCS}$ group of $\text{H}_2\text{BZmacropa-NCS}$ that is linked to a more electron-rich phenyl group. The increased stability of $\text{H}_2\text{BZmacropa-NCS}$ marks a potential advantage over $\text{H}_2\text{macropa-NCS}$, for $\text{H}_2\text{BZmacropa-NCS}$ may be shipped at room temperature and stored for extended periods of time, rendering it more broadly accessible to researchers across the globe.

Antibody Conjugation. To further evaluate the suitability of $\text{H}_2\text{BZmacropa-NCS}$ as a bifunctional chelator, this compound was conjugated to the antibody GC33, which targets the GPC3 receptor overexpressed in many liver cancers. The $\text{H}_2\text{BZmacropa-NCS}$ conjugate of GC33 (GC33-BZM) was prepared with standard antibody–isothiocyanate coupling conditions, which use a slight molar excess (2.5–3 equiv) of the chelator exposed to the antibody in bicarbonate buffer at 37°C . These conditions were also applied to prepare the macropa conjugate of GC33 (GC33-M) and the $\text{H}_2\text{BZmacropa-NCS}$ conjugate of obinutuzumab (OBI-BZM), an antibody that binds to human CD20 as a negative control. The conjugates were subjected to gel-permeation chromatography to remove any unconjugated bifunctional chelator, and their purities were verified using size-exclusion HPLC (Figures S52–S54).

After purification, the average chelator:antibody ratios were determined. Previous studies have shown that the presence of too many covalently attached chelators on antibodies can have negative consequences on their immunoreactivity and pharma-

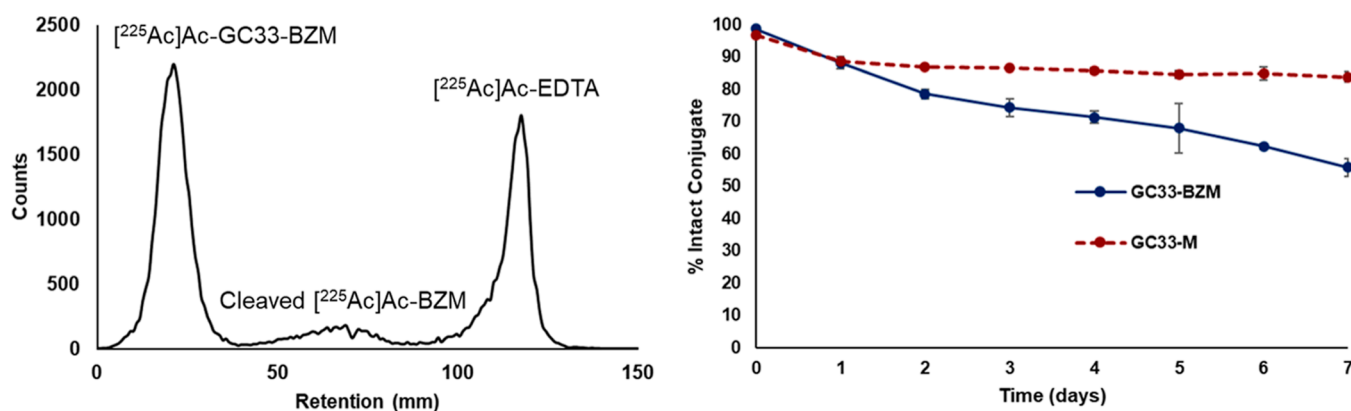
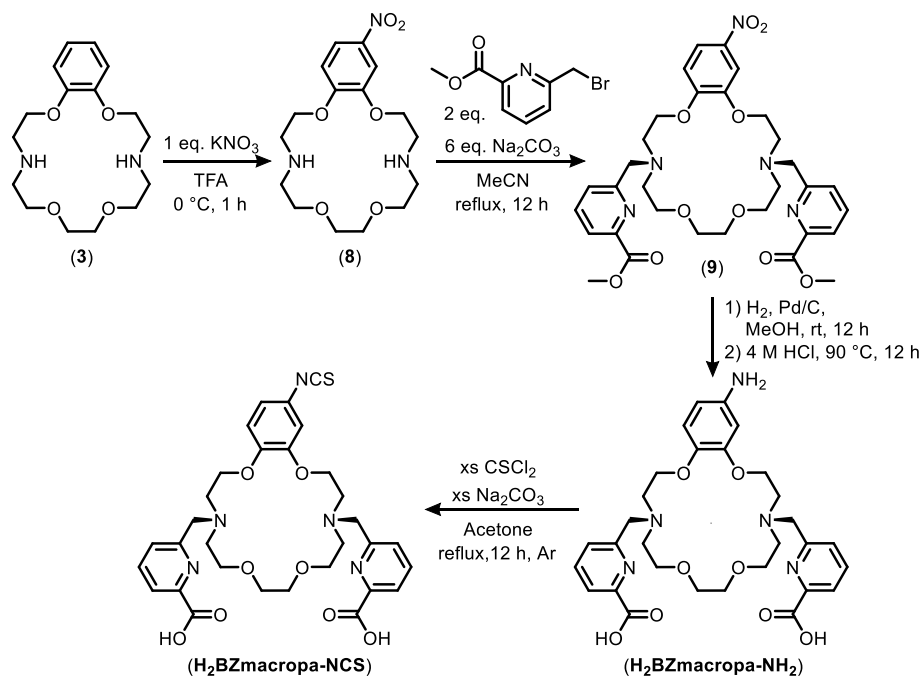
Scheme 1. Synthetic Scheme for H₂BZmacropa-NCS

Figure 3. (Left) ITLC chromatogram of [²²⁵Ac]Ac-GC33-BZM after 7 day incubation in human serum at 37 °C. (Right) Stability over time of [²²⁵Ac]Ac-GC33-BZM and [²²⁵Ac]Ac-GC33-M in human serum. Data points are the average of three independent samples, and error bars represent the standard deviation.

cokinetic properties. As such, a chelator:antibody ratio of <5 is generally desirable for radioconjugates.^{45–47} The chelator:antibody ratios were assessed using a modification of the previously reported colorimetric arsenazo assay (Figures S58–S59).⁴⁸ All conjugates were found to have chelator:antibody ratios of approximately 1:1 using this method, indicating that minimal alteration of the antibody was achieved. To provide further verification of these results, the chelator:antibody ratios of GC33-M and GC33-BZM were also determined using ultra-high-performance LC (UPLC)–high-resolution MS (HRMS). The resulting mass spectra, shown in Figures S55–S57, correspond well with the chelate:antibody ratios determined using the arsenazo method.

Having established the degree of functionalization of these conjugates, we next investigated the impact of this modification on the immunoreactivity of GC33 using bio-layer interferometry. The exposure of various concentrations of antibody–chelator conjugates to the immobilized GPC3 antigen showed concentration-dependent binding of the antibody to the surface

and subsequent dissociation. The combined association and dissociation kinetic data across all concentrations were fit using the global fitting model in Octet Analysis Studio software (Figures S60–S62). These data demonstrated *K*_d values of 0.19, 0.14, and 0.042 nM for GC33-BZM, GC33-M, and GC33, respectively. Taken together, the results show that both GC33-BZM and GC33-M retained comparably high binding affinity for GPC3, which was slightly diminished relative to that of the free GC33 antibody.

Radiolabeling and Stability Studies with Chelator–Antibody Conjugates. After confirming the identity, purity, and antigen-binding affinity of the antibody conjugates, they were radiolabeled with ²²⁵Ac following a previously reported procedure that was used for GC33-M.²⁹ Under these conditions, a solution of antibody conjugates (450 μg) was added to a solution of ²²⁵Ac (150 μCi, 5.55 MBq) in aqueous 0.1 M NH₄OAc (pH 5.5). The mixtures were incubated at room temperature for 30 min, after which the completion of the radiolabeling was checked using ITLC (Condition 2).

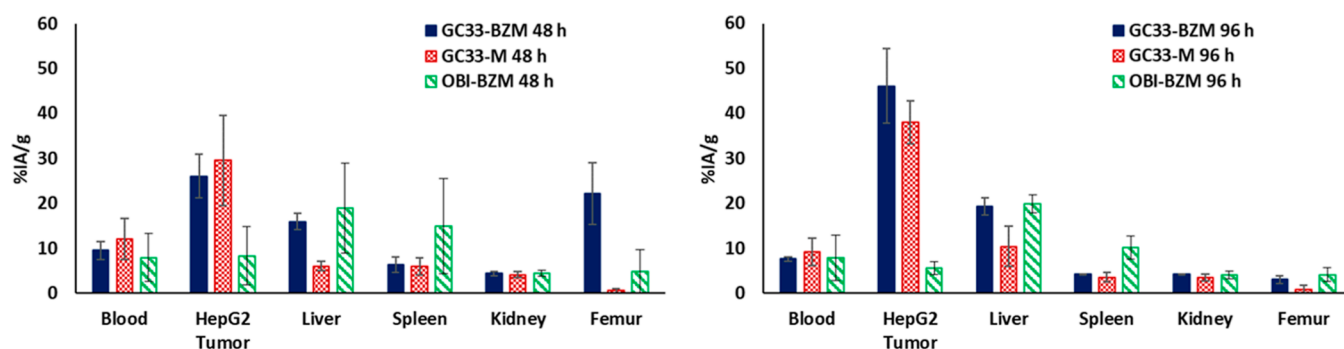


Figure 4. Selected organ biodistribution of ^{225}Ac -labeled GC33-BZM (solid, blue bar), ^{225}Ac -labeled GC33-M (checkered, red bar), and ^{225}Ac -labeled OBI-BZM (striped, green bar) at 48 h (left panel) and 96 h (right panel) after administration ($n = 3-4$). Full biodistribution data can be found in the Supporting Information, Figures S58–S60.

Purification of the radioconjugates via gel permeation chromatography afforded them in >95% purity, as verified by ITLC (Condition 2) (Figures S67–S69). The mild conditions and rapid reaction time required for these radiolabelings highlight the suitability of these chelators for antibody radioconjugates of ^{225}Ac . Importantly, the rapid room-temperature radiolabeling afforded by these conjugates is critical for minimizing radiolytic damage and thermal aggregation or denaturation of the antibody.

The stabilities of ^{225}Ac -GC33-BZM and ^{225}Ac -GC33-M were evaluated in whole human serum at 37 °C over several days (Figures 3 and S73–S74). Radio-ITLC analysis (Condition 2) confirmed that ^{225}Ac -GC33-M remained >90% intact over 7 days, highlighting the excellent stability of the ^{225}Ac complex of the bifunctional macropa-NCS²⁻ chelator. By contrast, radioconjugate ^{225}Ac -GC33-BZM exhibited marked degradation over the course of the experiment, with approximately 55% intact complex remaining after 7 days. The reduced stability of the ^{225}Ac -GC33-BZM conjugate relative to that of the unconjugated ligand- ^{225}Ac complex, which showed good stability in human serum, may arise from the electron-withdrawing effect of the thiourea moiety on the ligand backbone, which decreases its donating capacity. Notably, for both GC33-M and GC33-BZM radioconjugates, ITLC traces showed the presence of three distinct species in solution: intact conjugate, “free” ^{225}Ac chelated by the mobile phase EDTA, and a third unknown species. This third species reached approximately 10% of the total activity over the course of 1 day and then remained constant throughout the experiment. We hypothesize that this unknown product may be ^{225}Ac -macropa or ^{225}Ac -BZmacropa that has been cleaved from the antibody via radiolysis of the thiourea linker as extensive radiolysis is often observed in solutions containing ^{225}Ac .^{18,49}

Biodistribution Studies. Despite the lower stability of the ^{225}Ac -GC33-BZM conjugate relative to that of ^{225}Ac -GC33-M, we hypothesized that the former may still have sufficient stability for tumor targeting in vivo. To test whether ^{225}Ac -GC33-BZM could successfully target GPC3+ tumors in vivo, we treated athymic nude mice bearing HepG2 (GPC3+) xenografts with 100 nCi (3.7 kBq) of ^{225}Ac -GC33-BZM, ^{225}Ac -GC33-M (positive control), and ^{225}Ac -OBI-BZM (isotope control). After 48 and 96 h, mice ($n = 3-4$) were euthanized, and their organs were weighed and counted using a gamma counter after allowing 24 h for daughter isotope equilibration. The % injected activity per gram (IA/g) in each organ was then calculated (Figures 4, S75–S77). As expected, the isotope control ^{225}Ac -OBI-BZM, which does not target

the GPC3+ liver cancer xenografts, showed no appreciable tumor uptake at any time point. By contrast, ^{225}Ac -GC33-BZM demonstrated a clear, specific tumor uptake at both 48 and 96 h postinjection, with the tumor signal greater than that of all organs at both time points. Importantly, the tumor uptake of ^{225}Ac -GC33-BZM was effectively indistinguishable from that of ^{225}Ac -GC33-M, indicating that these conjugates have comparable targeting capabilities. However, the off-target accumulation of ^{225}Ac in both the liver and femur was higher after the administration of ^{225}Ac -GC33-BZM than for ^{225}Ac -GC33-M. A similar degree of liver uptake was also observed in the nontargeted isotype control conjugate ^{225}Ac -GC33-BZM. Unchelated ^{225}Ac has previously been shown to localize to the liver almost exclusively. Therefore, the higher liver uptake measured for both ^{225}Ac -GC33-BZM and ^{225}Ac -OBI-BZM may be a consequence of the partial instability of the ^{225}Ac -BZmacropa complex under these conditions.⁹ Despite these drawbacks, ^{225}Ac -GC33-BZM still demonstrates significant tumor uptake, suggesting that BZmacropa-NCS may be viable as a bifunctional chelator for in vivo studies of ^{225}Ac -labeled antibody conjugates.

CONCLUSIONS

In summary, two rigid variants of the first-generation ^{225}Ac chelator H₂macropa were synthesized by incorporating either one or two benzene rings into the macrocyclic base. Our comprehensive coordination chemistry studies of these ligands with La³⁺, a nonradioactive surrogate for Ac³⁺, confirmed that they form complexes that have lower stability than that of H₂macropa. DFT calculations were used to show that the use of phenyl groups in the backbone enhances their preorganization at the cost of their overall enthalpy of metal binding. These results highlight the different factors that need to be taken into consideration in designing and optimizing chelators for nuclear medicine applications. Despite their lower thermodynamic stability with La³⁺ when compared with H₂macropa, ^{225}Ac radiolabeling studies with these ligands proceeded effectively, yielding high-specific-activity compounds within minutes at room temperature. Thus, these chelators are among the few candidates that can bind ^{225}Ac under such mild conditions, rendering them valuable for use with temperature-sensitive macromolecular targeting vectors.

Based on these promising results, the bifunctional variant H₂BZmacropa-NCS was synthesized. In contrast to other large macrocyclic bifunctional chelators for ^{225}Ac , H₂BZmacropa-NCS places the reactive functional group directly on the

macrocycle rather than on the pendent arms. This design difference has two important implications. First, the synthetic approach is modular in that it allows for the installation of different pendent donor groups without perturbing the functional group handle on the macrocycle. Second, the stability of the –NCS functional group is substantially enhanced relative to that of the first-generation macropa-NCS. For this first-generation analogue, the –NCS group is installed on the pendent picolinate group and hydrolyzes rapidly in both the solid and solution states. These latter properties have made shipping and storage of this compound challenging. The enhanced hydrolytic stability of H₂BZmacropa-NCS, by contrast, should make it more accessible to other researchers. To further evaluate the suitability of this new bifunctional chelator, it was conjugated to antibody GC33, which can be employed for targeting liver cancers that express GPC3. Consistent with our expectations based on the small-molecule chelators, radiolabeling of the GC33-BZM proceeded rapidly under mild, room-temperature conditions. However, our serum stability and biodistribution studies showed ²²⁵Ac-labeled GC33-BZM to be less stable than the macropa conjugate yet still capable of delivering this radionuclide to the tumor site. Although the serum and in vivo stability of ²²⁵Ac-labeled GC33-BZM present some concerns, further optimization of this new bifunctional chelator, via modification of either the pendent donor arms or extension of the linker between the reactive –NCS group and the aromatic ring, may afford complexes of enhanced stability that are suitable for further clinical development. Alternatively, the use of H₂BZmacropa-NCS for other promising α -emitting radionuclides also warrants investigation. These efforts are currently underway within our labs.

■ ASSOCIATED CONTENT

SI Supporting Information

The Supporting Information is available free of charge at <https://pubs.acs.org/doi/10.1021/acs.bioconjchem.2c00190>.

Synthetic procedures, experimental details, NMR spectra, electrospray ionization HRMS spectra, direct analysis in real time MS spectra, HPLC chromatograms, hydrolysis of H₂BZmacropa-NCS in 0.1 M pH 9.1 Na₂CO₃/NaHCO₃ buffer at room temperature, pH potentiometric titration plots, calibration curves for the determination of chelate concentration, bio-layer interferometry analysis curves, ITLC chromatograms, and full ex vivo biodistribution histograms (PDF)

DFT-optimized geometries (ZIP)

X-ray crystal data of [La(BZmacropa)(H₂O)](PF₆) (CIF)

X-ray crystal data of [La(BZ₂macropa)(H₂O)](PF₆) (CIF)

■ AUTHOR INFORMATION

Corresponding Authors

Freddy E. Escorcia – Center for Cancer Research, National Cancer Institute, National Institutes of Health, Bethesda, Maryland 20892, United States; Phone: (240) 858-3062; Email: freddy.escorcia@nih.gov

Justin J. Wilson – Department of Chemistry and Chemical Biology, Cornell University, Ithaca, New York 14853, United States; orcid.org/0000-0002-4086-7982; Phone: (607) 255-4344; Email: jjw275@cornell.edu

Authors

Karthika J. Kadassery – Department of Chemistry and Chemical Biology, Cornell University, Ithaca, New York 14853, United States

A. Paden King – Center for Cancer Research, National Cancer Institute, National Institutes of Health, Bethesda, Maryland 20892, United States

Stanley Fayn – Center for Cancer Research, National Cancer Institute, National Institutes of Health, Bethesda, Maryland 20892, United States

Kwamena E. Baidoo – Center for Cancer Research, National Cancer Institute, National Institutes of Health, Bethesda, Maryland 20892, United States

Samantha N. MacMillan – Department of Chemistry and Chemical Biology, Cornell University, Ithaca, New York 14853, United States; orcid.org/0000-0001-6516-1823

Complete contact information is available at:

<https://pubs.acs.org/10.1021/acs.bioconjchem.2c00190>

Author Contributions

§K.J.K. and A.P.K. are equally contributing authors.

Notes

The authors declare the following competing financial interest(s): JJW and KJK are co-inventors on a provisional patent application on the use of the chelators reported in this manuscript for targeted alpha therapy applications.

■ ACKNOWLEDGMENTS

A.P.K., S.F., K.E.B., and F.E.E. acknowledge the support from the Intramural Research Program funds ZIA BC 011800 and ZIA BC 010891. K.J.K. and J.J.W. were supported by the Department of Energy Basic Energy Sciences (award no. DE-SC0021662) and National Institutes of Biomedical Imaging and Bioengineering of the National Institutes of Health (award numbers R21EB027282 and R01EB029259). J.J.W. also acknowledges the support from the Research Corporation for Science Advancement through a Cottrell Research Scholar Award. We are grateful to Chugai Pharmaceutical for providing codrituzumab (GC33).

■ REFERENCES

- (1) Parker, C.; Nilsson, S.; Heinrich, D.; Helle, S. I.; O'Sullivan, J. M.; Fossà, S. D.; Chodacki, A.; Wiechno, P.; Logue, J.; Seke, M.; et al. Alpha Emitter Radium-223 and Survival in Metastatic Prostate Cancer. *N. Engl. J. Med.* **2013**, *369*, 213–223.
- (2) Abou, D. S.; Thiele, N. A.; Gutsche, N. T.; Villmer, A.; Zhang, H.; Woods, J. J.; Baidoo, K. E.; Escorcia, F. E.; Wilson, J. J.; Thorek, D. L. J. Towards the Stable Chelation of Radium for Biomedical Applications with an 18-Membered Macrocyclic Ligand. *Chem. Sci.* **2021**, *12*, 3733–3742.
- (3) Nelson, B. J. B.; Andersson, J. D.; Wuest, F. Targeted Alpha Therapy: Progress in Radionuclide Production, Radiochemistry, and Applications. *Pharmaceutics* **2021**, *13*, 49.
- (4) King, A. P.; Lin, F. I.; Escorcia, F. E. Why Bother with Alpha Particles? *Eur. J. Nucl. Med. Mol. Imaging* **2021**, *49*, 7–17.
- (5) Thiele, N. A.; Wilson, J. J. Actinium-225 for Targeted α Therapy: Coordination Chemistry and Current Chelation Approaches. *Cancer Biother. Radiopharm.* **2018**, *33*, 336–348.
- (6) Yadav, M. P.; Ballal, S.; Sahoo, R. K.; Tripathi, M.; Seth, A.; Bal, C. Efficacy and Safety of ²²⁵Ac-PSMA-617 Targeted Alpha Therapy in Metastatic Castration-Resistant Prostate Cancer Patients. *Theranostics* **2020**, *10*, 9364–9377.
- (7) Ballal, S.; Yadav, M. P.; Bal, C.; Sahoo, R. K.; Tripathi, M. Broadening Horizons with ²²⁵Ac-DOTATATE Targeted Alpha

- Therapy for Gastroenteropancreatic Neuroendocrine Tumour Patients Stable or Refractory to ^{177}Lu -DOTATATE PRRT: First Clinical Experience on the Efficacy and Safety. *Eur. J. Nucl. Med. Mol. Imaging* **2020**, *47*, 934–946.
- (8) Tagawa, S. T.; Sun, M.; Sartor, A. O.; Thomas, C.; Singh, S.; Bissassar, M.; Fernandez, E.; Niaz, M. J.; Ho, B.; Vallabhajosula, S.; et al. Phase I Study of ^{225}Ac -J591 for Men with Metastatic Castration-Resistant Prostate Cancer (mCRPC). *J. Clin. Oncol.* **2021**, *39*, 5015.
- (9) Davis, I. A.; Glowienka, K. A.; Boll, R. A.; Deal, K. A.; Brechbiel, M. W.; Stabin, M.; Bochsler, P. N.; Mirzadeh, S.; Kennel, S. J. Comparison of ^{225}Ac Actinium Chelates: Tissue Distribution and Radiotoxicity. *Nucl. Med. Biol.* **1999**, *26*, 581–589.
- (10) Maguire, W. F.; McDevitt, M. R.; Smith-Jones, P. M.; Scheinberg, D. A. Efficient 1-Step Radiolabeling of Monoclonal Antibodies to High Specific Activity with ^{225}Ac for α -Particle Radioimmunotherapy of Cancer. *J. Nucl. Med.* **2014**, *55*, 1492–1498.
- (11) Mesude, B.; Katharina, L.; Teja, K.; Phelps, M. E.; Strand, S.; Morris, M. J.; Radu, C. G.; Damoiseaux, R.; Peltola, M. T.; Peekhaus, N.; et al. Genetic Signature of Prostate Cancer Mouse Models Resistant to Optimized HK2 Targeted α -Particle Therapy. *Proc. Natl. Acad. Sci. U.S.A.* **2020**, *117*, 15172–15181.
- (12) Lakes, A. L.; An, D. D.; Gauny, S. S.; Ansoborlo, C.; Liang, B. H.; Rees, J. A.; McKnight, K. D.; Karsunky, H.; Abergel, R. J. Evaluating ^{225}Ac and ^{177}Lu Radioimmunoconjugates against Antibody–Drug Conjugates for Small-Cell Lung Cancer. *Mol. Pharm.* **2020**, *17*, 4270–4279.
- (13) Sudo, H.; Tsuji, A. B.; Sugyo, A.; Kaneko, M. K.; Kato, Y.; Nagatsu, K.; Suzuki, H.; Higashi, T. Preclinical Evaluation of Podoplanin-Targeted Alpha-Radioimmunotherapy with the Novel Antibody NZ-16 for Malignant Mesothelioma. *Cells* **2021**, *10*, 2503.
- (14) Sudo, H.; Tsuji, A. B.; Sugyo, A.; Harada, Y.; Nagayama, S.; Katagiri, T.; Nakamura, Y.; Higashi, T. FZD10-Targeted α -Radioimmunotherapy with ^{225}Ac -Labeled OTSA101 Achieves Complete Remission in a Synovial Sarcoma Model. *Cancer Sci.* **2022**, *113*, 721–732.
- (15) Ramogida, C. F.; Robertson, A. K. H.; Jermilova, U.; Zhang, C.; Yang, H.; Kunz, P.; Lassen, J.; Bratanovic, I.; Brown, V.; Southcott, L.; et al. Evaluation of Polydentate Picolinic Acid Chelating Ligands and an α -Melanocyte-Stimulating Hormone Derivative for Targeted Alpha Therapy Using ISOL-Produced ^{225}Ac . *EJNMMI Radiopharm. Chem.* **2019**, *4*, 21.
- (16) Deal, K. A.; Davis, I. A.; Mirzadeh, S.; Kennel, S. J.; Brechbiel, M. W. Improved in Vivo Stability of Actinium-225 Macrocylic Complexes. *J. Med. Chem.* **1999**, *42*, 2988–2992.
- (17) Comba, P.; Jermilova, U.; Orvig, C.; Patrick, B. O.; Ramogida, C. F.; Rück, K.; Schneider, C.; Starke, M. Octadentate Picolinic Acid-Based Bispidine Ligand for Radiometal Ions. *Chem. - Eur. J.* **2017**, *23*, 15945–15956.
- (18) Yang, H.; Zhang, C.; Yuan, Z.; Rodriguez-Rodriguez, C.; Robertson, A.; Radchenko, V.; Perron, R.; Gendron, D.; Causey, P.; Gao, F.; et al. Synthesis and Evaluation of a Macrocylic Actinium-225 Chelator, Quality Control and In Vivo Evaluation of ^{225}Ac -Crown-AMSH Peptide. *Chem. - Eur. J.* **2020**, *26*, 11435–11440.
- (19) Hu, A.; Brown, V.; MacMillan, S. N.; Radchenko, V.; Yang, H.; Wharton, L.; Ramogida, C. F.; Wilson, J. J. Chelating the Alpha Therapy Radionuclides $^{225}\text{Ac}^{3+}$ and $^{213}\text{Bi}^{3+}$ with 18-Membered Macrocylic Ligands MacroDipa and Py-MacroDipa. *Inorg. Chem.* **2022**, *61*, 801–806.
- (20) Li, L.; Rousseau, J.; Jaraquemada-Peláez, M. d. G.; Wang, X.; Robertson, A.; Radchenko, V.; Schaffer, P.; Lin, K.-S.; Bénard, F.; Orvig, C. ^{225}Ac -H₄Py4pa for Targeted Alpha Therapy. *Bioconjugate Chem.* **2021**, *32*, 1348–1363.
- (21) Roca-Sabio, A.; Mato-Iglesias, M.; Esteban-Gómez, D.; Tóth, É.; Blas, A. d.; Platas-Iglesias, C.; Rodríguez-Blas, T. Macrocylic Receptor Exhibiting Unprecedented Selectivity for Light Lanthanides. *J. Am. Chem. Soc.* **2009**, *131*, 3331–3341.
- (22) Clarke, E. T.; Martell, A. E. Stabilities of Trivalent Metal Ion Complexes of the Tetraacetate Derivatives of 12-, 13- and 14-Membered Tetraazamacrocycles. *Inorg. Chim. Acta* **1991**, *190*, 37–46.
- (23) Smith, R. M.; Martell, A. E. *Critical Stability Constants*; Plenum Press: New York; London, 1974; Vol. 1.
- (24) Thiele, N. A.; Brown, V.; Kelly, J. M.; Amor-Coarasa, A.; Jermilova, U.; MacMillan, S. N.; Nikolopoulou, A.; Ponnala, S.; Ramogida, C. F.; Robertson, A. K. H.; et al. An Eighteen-Membered Macrocylic Ligand for Actinium-225 Targeted Alpha Therapy. *Angew. Chem., Int. Ed.* **2017**, *56*, 14712–14717.
- (25) Hu, A.; Wilson, J. J. Advancing Chelation Strategies for Large Metal Ions for Nuclear Medicine Applications. *Acc. Chem. Res.* **2022**, *55*, 904–915.
- (26) Kelly, J. M.; Amor-Coarasa, A.; Ponnala, S.; Nikolopoulou, A.; Williams, C.; Thiele, N. A.; Schlyer, D.; Wilson, J. J.; DiMaggio, S. G.; Babich, J. W. A Single Dose of ^{225}Ac -RPS-074 Induces a Complete Tumor Response in an LNCaP Xenograft Model. *J. Nucl. Med.* **2019**, *60*, 649–655.
- (27) Aluicio-Sarduy, E.; Thiele, N. A.; Martin, K. E.; Vaughn, B. A.; Devaraj, J.; Olson, A. P.; Barnhart, T. E.; Wilson, J. J.; Boros, E.; Engle, J. W. Establishing Radiolanthanum Chemistry for Targeted Nuclear Medicine Applications. *Chem. - Eur. J.* **2020**, *26*, 1238–1242.
- (28) Reissig, F.; Bauer, D.; Zarschler, K.; Novy, Z.; Bendova, K.; Ludik, M.-C.; Kopka, K.; Pietzsch, H.-J.; Petrik, M.; Mamat, C. Towards Targeted Alpha Therapy with Actinium-225: Chelators for Mild Condition Radiolabeling and Targeting PSMA—A Proof of Concept Study. *Cancers* **2021**, *13*, 1974.
- (29) Bell, M. M.; Gutsche, N. T.; King, A. P.; Baidoo, K. E.; Kelada, O. J.; Choyke, P. L.; Escorcía, F. E. Glypican-3-Targeted Alpha Particle Therapy for Hepatocellular Carcinoma. *Molecules* **2021**, *26*, 4.
- (30) De Sousa, A. S.; Croft, G. J. B.; Wagner, C. A.; Michael, J. P.; Hancock, R. D. Effect of Cyclohexylene Bridges on the Metal Ion Size Based Selectivity of Ligands in Aqueous Solution. *Inorg. Chem.* **1991**, *30*, 3525–3529.
- (31) Brechbiel, M. W.; Gansow, O. A. Synthesis of C-Functionalized Trans-Cyclohexyldiethylenetriaminepenta-Acetic Acids for Labelling of Monoclonal Antibodies with the Bismuth-212 α -Particle Emitter. *J. Chem. Soc., Perkin Trans.* **1992**, *19*, 1173–1178.
- (32) Ferreirós-Martínez, R.; Esteban-Gómez, D.; Platas-Iglesias, C.; de Blas, A.; Rodríguez-Blas, T. Zn(II), Cd(II) and Pb(II) Complexation with Pyridinecarboxylate Containing Ligands. *Dalton Trans.* **2008**, *42*, 5754–5765.
- (33) Ramogida, C. F.; Cawthray, J. F.; Boros, E.; Ferreira, C. L.; Patrick, B. O.; Adam, M. J.; Orvig, C. H₂CHXDeDpa and H₄CHXOctapa—Chiral Acyclic Chelating Ligands for $^{67/68}\text{Ga}$ and ^{111}In Radiopharmaceuticals. *Inorg. Chem.* **2015**, *54*, 2017–2031.
- (34) Wang, X.; Jaraquemada-Peláez, M. d. G.; Cao, Y.; Ingham, A.; Rodríguez-Rodríguez, C.; Pan, J.; Wang, Y.; Saatchi, K.; Häfeli, U. O.; Lin, K.-S.; et al. H₂CHXHox: Rigid Cyclohexane-Reinforced Non-macrocylic Chelating Ligand for [^{225}Ac] $^{3+}$. *Inorg. Chem.* **2020**, *59*, 4895–4908.
- (35) Hu, A.; Aluicio-Sarduy, E.; Brown, V.; MacMillan, S. N.; Becker, K. V.; Barnhart, T. E.; Radchenko, V.; Ramogida, C. F.; Engle, J. W.; Wilson, J. J. A Janus Chelator Capable of Binding Medicinally Relevant Rare-Earth Radiometals of Disparate Sizes. *J. Am. Chem. Soc.* **2021**, *143*, 10429–10440.
- (36) Ishiguro, T.; Sugimoto, M.; Kinoshita, Y.; Miyazaki, Y.; Nakano, K.; Tsunoda, H.; Sugo, I.; Ohizumi, I.; Aburatani, H.; Hamakubo, T.; Kodama, T.; Tsuchiya, M.; Yamada-Okabe, H. Anti-Glypican 3 Antibody as a Potential Antitumor Agent for Human Liver Cancer. *Cancer Res.* **2008**, *68*, 9832–9838.
- (37) Panchenko, P. A.; Zubenko, A. D.; Chernikova, E. Y.; Fedorov, Y. V.; Pashanova, A. V.; Karnoukhova, V. A.; Fedyanin, I. V.; Fedorova, O. A. Synthesis, Structure and Metal Ion Coordination of Novel Benzodiazamacrocyclic Ligands Bearing Pyridyl and Picolinate Pendant Side-Arms. *New J. Chem.* **2019**, *43*, 15072–15086.
- (38) Thiele, N. A.; Woods, J. J.; Wilson, J. J. Implementing f-Block Metal Ions in Medicine: Tuning the Size Selectivity of Expanded Macrocylics. *Inorg. Chem.* **2019**, *58*, 10483–10500.
- (39) Deblonde, G. J.-P.; Zavarin, M.; Kersting, A. B. The Coordination Properties and Ionic Radius of Actinium: A 120-Year-Old Enigma. *Coord. Chem. Rev.* **2021**, *446*, 214130.

- (40) Corbaux, P.; Spiess, B.; Arnaud, F.; Schwing, M. J. Complexing Properties of an N,N'-Methylated Diaza-Crown-Ether. *Polyhedron* **1985**, *4*, 1471–1473.
- (41) Fedorova, O.; Fedorov, Y.; Oshchepkov, M. Complexes of Di- and Triazacrown Ethers with Heavy Metal Ions in Water Solution. *Electroanalysis* **2012**, *24*, 1739–1744.
- (42) Tei, L.; Baranyai, Z.; Botta, M.; Piscopo, L.; Aime, S.; Giovenzana, G. B. Synthesis and Solution Thermodynamic Study of Rigidified and Functionalised EGTA Derivatives. *Org. Biomol. Chem.* **2008**, *6*, 2361–2368.
- (43) Wilson, J. J.; Ferrier, M.; Radchenko, V.; Maassen, J. R.; Engle, J. W.; Batista, E. R.; Martin, R. L.; Nortier, F. M.; Fassbender, M. E.; John, K. D.; et al. Evaluation of Nitrogen-Rich Macrocyclic Ligands for the Chelation of Therapeutic Bismuth Radioisotopes. *Nucl. Med. Biol.* **2015**, *42*, 428–438.
- (44) Hu, A.; MacMillan, S. N.; Wilson, J. J. Macrocyclic Ligands with an Unprecedented Size-Selectivity Pattern for the Lanthanide Ions. *J. Am. Chem. Soc.* **2020**, *142*, 13500–13506.
- (45) Vosjan, M. J. W. D.; Perk, L. R.; Visser, G. W. M.; Budde, M.; Jurek, P.; Kiefer, G. E.; van Dongen, G. A. M. S. Conjugation and Radiolabeling of Monoclonal Antibodies with Zirconium-89 for PET Imaging Using the Bifunctional Chelate p-Isothiocyanatobenzyl-Desferrioxamine. *Nat. Protoc.* **2010**, *5*, 739–743.
- (46) Al-Ejeh, F.; Darby, J. M.; Thierry, B.; Brown, M. P. A Simplified Suite of Methods to Evaluate Chelator Conjugation of Antibodies: Effects on Hydrodynamic Radius and Biodistribution. *Nucl. Med. Biol.* **2009**, *36*, 395–402.
- (47) Sharma, S. K.; Glaser, J. M.; Edwards, K. J.; Khozeimeh Sarbisheh, E.; Salih, A. K.; Lewis, J. S.; Price, E. W. A Systematic Evaluation of Antibody Modification and ⁸⁹Zr-Radiolabeling for Optimized Immuno-PET. *Bioconjugate Chem.* **2021**, *32*, 1177–1191.
- (48) Dadachova, E.; Chappell, L. L.; Brechbiel, M. W. Spectrophotometric Method for Determination of Bifunctional Macrocyclic Ligands in Macrocyclic Ligand–Protein Conjugates. *Nucl. Med. Biol.* **1999**, *26*, 977–982.
- (49) Hooijman, E. L.; Chalashkan, Y.; Ling, S. W.; Kahyargil, F. F.; Segbers, M.; Bruchertseifer, F.; Morgenstern, A.; Seimbille, Y.; Koolen, S. L. W.; Brabander, T.; et al. Development of [²²⁵Ac]Ac-PSMA-I&T for Targeted Alpha Therapy According to GMP Guidelines for Treatment of mCRPC. *Pharmaceutics* **2021**, *13*, 715.

Recommended by ACS

Development of Bispecific NT-PSMA Heterodimer for Prostate Cancer Imaging: A Potential Approach to Address Tumor Heterogeneity

Xiaofen Ma, Zibo Li, *et al.*

APRIL 29, 2019
BIOCONJUGATE CHEMISTRY

READ 

Quantitative Imaging of Tumor-Associated Macrophages and Their Response to Therapy Using ⁶⁴Cu-Labeled Macrin

Hye-Yeong Kim, Miles A. Miller, *et al.*

DECEMBER 03, 2018
ACS NANO

READ 

Quantitative ^{99m}Tc Labeling Kit for HYNIC-Conjugated Single Chain Antibody Fragments Targeting Malignant Mesothelioma

Jiang He, Bin Liu, *et al.*

JULY 06, 2020
BIOCONJUGATE CHEMISTRY

READ 

Toward Understanding the Binding Synergy of Trastuzumab and Pertuzumab to Human Epidermal Growth Factor Receptor 2

Rohit Sharma, Archana Mukherjee, *et al.*

NOVEMBER 10, 2021
MOLECULAR PHARMACEUTICS

READ 

Get More Suggestions >